

A first-principles study on the B₅O₅ +/0 and B₅O₅ - clusters: The boron oxide analogs of C₆H₅ +/0 and CH₃Cl

Wen-Juan Tian, Xue-Rui You, Da-Zhi Li, Ting Ou, Qiang Chen, Hua-Jin Zhai, and Si-Dian Li

Citation: *The Journal of Chemical Physics* **143**, 064303 (2015); doi: 10.1063/1.4928282

View online: <http://dx.doi.org/10.1063/1.4928282>

View Table of Contents: <http://scitation.aip.org/content/aip/journal/jcp/143/6?ver=pdfcov>

Published by the AIP Publishing

Articles you may be interested in

Highly stable and symmetric boron caged B @ Co 12 @ B 80 core-shell cluster
Appl. Phys. Lett. **94**, 133102 (2009); 10.1063/1.3111444

Theoretical study of structure and photoelectron spectroscopy of In x P y - and In x P y (x + y = 6) clusters
J. Chem. Phys. **124**, 184316 (2006); 10.1063/1.2194553

Structure of the Na x Cl x+1 - (x=1–4) clusters via ab initio genetic algorithm and photoelectron spectroscopy
J. Chem. Phys. **121**, 5709 (2004); 10.1063/1.1783276

Products of the addition of water molecules to Al 3 O 3 - clusters: Structure, bonding, and electron binding energies in Al 3 O 4 H 2 - , Al 3 O 5 H 4 - , Al 3 O 4 H 2 , and Al 3 O 5 H 4
J. Chem. Phys. **120**, 7955 (2004); 10.1063/1.1689648

A study of the structure and bonding of small aluminum oxide clusters by photoelectron spectroscopy: Al x O y - (x=1–2, y=1–5)
J. Chem. Phys. **106**, 1309 (1997); 10.1063/1.474085



NEW Special Topic Sections

NOW ONLINE
Lithium Niobate Properties and Applications:
Reviews of Emerging Trends

**AIP | Applied Physics
Reviews**

A first-principles study on the $B_5O_5^{+/0}$ and $B_5O_5^-$ clusters: The boron oxide analogs of $C_6H_5^{+/0}$ and CH_3Cl

Wen-Juan Tian,¹ Xue-Rui You,¹ Da-Zhi Li,² Ting Ou,¹ Qiang Chen,¹ Hua-Jin Zhai,^{1,3,a)} and Si-Dian Li^{1,b)}

¹Nanocluster Laboratory, Institute of Molecular Science, Shanxi University, Taiyuan 030006, China

²Department of Chemistry and Chemical Engineering, Binzhou University, Binzhou 256603, China

³State Key Laboratory of Quantum Optics and Quantum Optics Devices, Shanxi University, Taiyuan 030006, China

(Received 8 June 2015; accepted 28 July 2015; published online 12 August 2015)

The concept of boronyl (BO) and the BO/H isolobal analogy build an interesting structural link between boron oxide clusters and hydrocarbons. Based upon global-minimum searches and first-principles electronic structural calculations, we present here the perfectly planar $C_{2v} B_5O_5^+$ (**1**, 1A_1), $C_{2v} B_5O_5$ (**2**, 2A_1), and tetrahedral $C_s B_5O_5^-$ (**3**, ${}^1A'$) clusters, which are the global minima of the systems. Structural and molecular orbital analyses indicate that $C_{2v} B_5O_5^+$ (**1**) [$B_3O_3(BO)_2^+$] and $C_{2v} B_5O_5$ (**2**) [$B_3O_3(BO)_2$] feature an aromatic six-membered boroxol (B_3O_3) ring as the core with two equivalent boronyl terminals, similar to the recently reported boronyl boroxine $D_{3h} B_6O_6$ [$B_3O_3(BO)_3$]; whereas $C_s B_5O_5^-$ (**3**) [$B(BO)_3(OBO)^-$] is characterized with a tetrahedral B^- center, terminated with three BO groups and one OBO unit, similar to the previously predicted boronyl methane $T_d B_5O_4^-$ [$B(BO)_4^-$]. Alternatively, the **1–3** clusters can be viewed as the boron oxide analogs of phenyl cation $C_6H_5^+$, phenyl radical C_6H_5 , and chloromethane CH_3Cl , respectively. Chemical bonding analyses also reveal a dual three-center four-electron (3c-4e) π hyperbond in $C_s B_5O_5^-$ (**3**). The infrared absorption spectra of $B_5O_5^+$ (**1**), B_5O_5 (**2**), and $B_5O_5^-$ (**3**) and anion photoelectron spectrum of $B_5O_5^-$ (**3**) are predicted to facilitate their forthcoming experimental characterizations. The present work completes the $B_nO_n^{+/0/-}$ series for $n = 1–6$ and enriches the analogous relationship between boron oxides and hydrocarbons. © 2015 AIP Publishing LLC. [http://dx.doi.org/10.1063/1.4928282]

I. INTRODUCTION

As the prototype of electron-deficient elements, boron has a rich chemistry, which leads to unusual structural and electronic properties and novel chemical bonding patterns for elemental boron clusters.^{1–25} A number of recent studies have revealed the analogy between bare boron clusters and hydrocarbons, including polycyclic aromatic hydrocarbons (PAHs). The B_8^{2-} , B_9^- , B_{10} , B_{11}^- , B_{12} , and B_{13}^+ clusters are all 6 π aromatic systems and can be viewed as the inorganic analogs of benzene,^{5,7,13} whereas B_{16}^{2-} , B_{22}^- , and B_{23}^- clusters are all-boron analogs of naphthalene, anthracene, and phenanthrene, respectively.^{8,15} Furthermore, the analogous relationship between boron hydrides and hydrocarbons has been demonstrated.^{26,27} Very recently, a new member of the “inorganic benzene” family, $D_{3h} B_6O_6$ (that is, boronyl boroxine), has been discovered computationally,²⁸ which is a boron oxide analog of boroxine ($B_3O_3H_3$). The B_6O_6 cluster has a boroxol (B_3O_3) ring as the structural core and shares the same π bonding pattern as C_6H_6 and $B_3O_3H_3$.

A variety of boron oxide clusters have been studied in the past years, indicating the key role of the boronyl (BO) group in determining their global-minimum structures and the nature

of bonding.^{28–48} Among the existing understanding, the majority of theoretical studies are carried out on boron-rich boron oxide clusters. Relatively little is known about the oxygen-rich B_nO_m clusters and those with equal content of boron and oxygen ($n \leq m$), which should offer opportunities to explore exotic chemical bonding. As for the B_nO_n clusters, $B_3O_3^{-/0/+}$, $B_4O_4^{-/0}$, and $B_6O_6^{-/0}$ were studied in our recent works.^{28,46,48} The $T_d B_5O_4^-$ [$B(BO)_4^-$] and $D_{3h} B_6O_6$ [$B_3O_3(BO)_3$] species are “magic” clusters^{28,44} with perfect B versus O compositions, consistent with their high symmetries and extraordinary stabilities. Obviously, the $B_5O_5^{+/0/-}$ clusters are less than ideal in terms of the B/O compositions, and their global-minimum structures and chemical bonding are still unknown. However, such clusters can provide valuable model systems to elucidate the interplay and competition between the $B\equiv O$, OBO, boroxol B_3O_3 ring, and BB bonding in the boron oxide clusters and to demonstrate how a single charge can change the global-minimum structures drastically.

In the current contribution, we have carried out detailed structural searches and electronic structure calculations for the $B_5O_5^+$, B_5O_5 , and $B_5O_5^-$ clusters. We report their global-minimum structures and chemical bonding patterns. Our results show that the $B_5O_5^+$ and B_5O_5 species share nearly the same architecture that consists of a boroxol B_3O_3 ring and two terminal BO units, which can be alternatively formulated as $B_3O_3(BO)_2^+$ (**1**, C_{2v} , 1A_1) and $B_3O_3(BO)_2$ (**2**, C_{2v} , 2A_1),

a)Electronic mail: hj.zhai@sxu.edu.cn

b)Electronic mail: lisidian@sxu.edu.cn

respectively. These are boron oxide analogs of the organic phenyl cation and phenyl radical, $C_6H_5^{+/0}$, which are all perfectly planar with an aromatic π sextet, akin to benzene. On the other hand, the $B_5O_5^-$ anion cluster possesses a three-dimensional global-minimum structure, which is characterized with a tetrahedral B^- center attached by three BO groups and one OBO unit. This anion can be formulated as $B(BO)_3(OBO)^-$ (**3**, C_s , $^1A'$); it is readily constructed from T_d $B(BO)_4^-$ via the substitution of one terminal BO by an OBO.⁴⁴ Due to the BO/H isolobal analogy (both are monovalent σ radicals)²⁹ and the fact that an OBO unit is a typical superhalogen,³³ the $B_5O_5^-$ (**3**, C_s , $^1A'$) cluster may be considered as a boron oxide analog of chloromethane or methylchloride (CH_3Cl). The above-mentioned analogies to organic molecules are firmly established through chemical bonding analyses. To facilitate their experimental characterizations, the infrared (IR) absorption spectra of $B_5O_5^+$ (**1**), B_5O_5 (**2**), and $B_5O_5^-$ (**3**) and anion photoelectron spectrum of $B_5O_5^-$ (**3**) are predicted computationally. The current results complete the $B_nO_n^{+/0/-}$ series ($n = 1-6$) and enrich the analogous relationship between boron oxides and hydrocarbons.

II. THEORETICAL METHODS

The global-minimum structural searches for $B_5O_5^{+/0/-}$ clusters were conducted at the density-functional theory (DFT) level using the Coalescence Kick (CK)^{49,50} program, aided with manual structural constructions. The candidate low-lying structures were fully optimized at the B3LYP/aug-cc-pVTZ level.⁵¹ Harmonic vibrational frequencies were calculated at

the same level to verify that the reported structures are true minima. Single-point coupled-cluster calculations (CCSD(T))⁵²⁻⁵⁴ were done at the B3LYP geometries to further evaluate the relative energies of the top low-lying structures within 40 kcal/mol in different charge states. Adaptive natural density partitioning (AdNDP)⁵⁵ and canonical molecular orbital (CMO) analyses were performed to understand the chemical bonding patterns. Natural bond orbital (NBO) analysis was carried out to get the natural atomic charges and the Wiberg bond indices.⁵⁶ Photoelectron spectrum of global-minimum $B_5O_5^-$ anion cluster was simulated at the time-dependent B3LYP (TD-B3LYP)^{57,58} level, along with the predicted IR spectra of the $B_5O_5^{+/0/-}$ clusters. The AdNDP analyses were performed using the AdNDP program⁵⁵ and all other calculations and analyses were performed using the Gaussian 09 package.⁵⁹

III. RESULTS

Global-minimum searches using the CK program have identified the low-lying isomeric structures for $B_5O_5^{+/0/-}$, which are fully reoptimized subsequently at the B3LYP/aug-cc-pVTZ level.⁵¹ The cluster structures are collected in the supplementary material as Figs. S1–S3,⁶⁰ along with their relative energies. The relative energies for top low-lying structures within 40 kcal/mol are further refined at the single-point CCSD(T)/B3LYP/aug-cc-pVTZ level. The relative energies and vibrational frequencies for key relevant structures of $B_5O_5^{+/0/-}$ are listed in Table I. The global minima of $B_5O_5^{+/0/-}$ clusters are all reasonably well-defined from their nearest

TABLE I. Relative energies and vibrational frequencies for all optimized planar and tetrahedral isomeric structures of $B_5O_5^{+/0/-}$ clusters at the B3LYP/aug-cc-pVTZ level.

Charge state	Cation ^a		Neutral		Anion	
	Relative energy (kcal/mol)	Frequency (cm^{-1}) ^b	Relative energy (kcal/mol)	Frequency (cm^{-1}) ^b	Relative energy (kcal/mol)	Frequency (cm^{-1}) ^b
	0.00	0.00	0.00	0.00	0.00	0.00
Frequency (cm^{-1}) ^b	77 (a_1) 79 (b_1) 284 (b_1) 418 (a_1) 472 (b_2) 509 (b_1) 550 (a_1) 660 (b_1) 736 (a_1) 884 (b_2) 1017 (a_1) 1178 (a_1) 1337 (b_2) 1840 (b_2)	79 (b_1) 81 (a_1) 152 (b_2) 263 (b_1) 368 (b_1) 444 (a_1) 498 (b_2) 596 (a_1) 694 (b_1) 702 (b_2) 1096 (a_1) 1196 (a_1) 1199 (b_2) 1350 (a_1) 1367 (b_2) 2026 (b_2) 2027 (a_1) 2046 (a')	68 (a'') 86 (a') 132 (a') 143 (a'') 192 (a') 358 (a'') 381 (a') 387 (a') 473 (a') 496 (a'') 523 (a'') 529 (a') 843 (a') 1308 (a') 1907 (a'') 1942 (a') 1987 (a') 2046 (a')	103 (a') 192 (a') 433 (a') 435 (a'') 494 (a') 520 (a') 525 (a'') 532 (a'') 578 (a') 821 (a') 1187 (a') 1926 (a') 1926 (a'') 1941 (a') 2043 (a') 2046 (a')	136 (b_1) 153 (b_2) 347 (b_1) 451 (a_1) 497 (b_2) 681 (b_2) 697 (b_1) 727 (b_2) 756 (a_1) 885 (a_1) 1144 (a_1) 1239 (b_2) 1408 (a_1) 1970 (b_2) 1971 (a_1)	

^aFor the cationic charge state, the CH_3Cl -like structure dissociates during the structural optimization.

^bFrequencies with intensities of less than 5.0 km/mol are not shown.

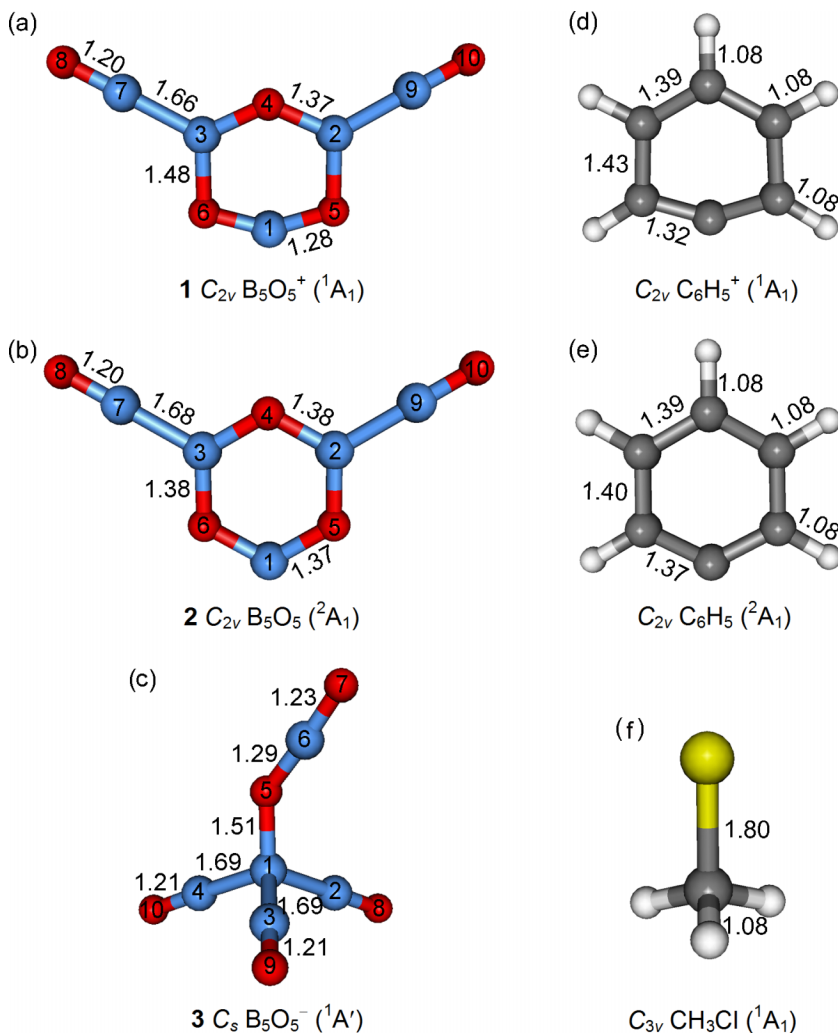


FIG. 1. Optimized global-minimum structures of $\text{B}_5\text{O}_5^{+/0-}$ (**1–3**) at the B3LYP/aug-cc-pVTZ level, as compared to those of $\text{C}_6\text{H}_5^{+/0}$ and CH_3Cl . Bond distances (in Å) are indicated. The B atom is in blue, O in red, C in thick gray, and H in light gray.

alternative isomer, and thus the zero-point energy (ZPE) corrections were not pursued. For $\text{B}_5\text{O}_5^{+/0}$ clusters, the global minima B_5O_5^+ (**1**, C_{2v} , ${}^1\text{A}_1$) and B_5O_5 (**2**, C_{2v} , ${}^2\text{A}_1$) (Fig. 1) are at least 16 kcal/mol lower in energy at the B3LYP level, which are refined to at least 12 kcal/mol at the single-point CCSD(T) level.

The potential energy surface for the B_5O_5^- anion cluster is slightly more complicated (supplementary Fig. S3).⁶⁰ The global minimum B_5O_5^- (**3**, C_s , ${}^1\text{A}'$) (Fig. 1) is followed by a competitive isomer, (C_{2v} , ${}^1\text{A}_1$), which is about 6 kcal/mol above the global minimum at the B3LYP level, further refined to about 2 kcal/mol at the single-point CCSD(T) level. However, beyond these two structures, all other isomers are significantly higher in energy, by at least 12 kcal/mol (supplementary Fig. S3).⁶⁰ The competitive (C_{2v} , ${}^1\text{A}_1$) isomer is thus also an important structure for the B_5O_5^- anion.

Detailed structures and bond distances for the global minima of $\text{B}_5\text{O}_5^{+/0-/-}$ (**1–3**) at the B3LYP level are illustrated in Fig. 1; also shown are those of their hydrocarbon counterparts. The global minima of the $\text{B}_5\text{O}_5^{+/0}$ clusters are **1** (C_{2v} , ${}^1\text{A}_1$) and **2** (C_{2v} , ${}^2\text{A}_1$), respectively, which both contain one B_3O_3 ring and two terminal BO groups (Fig. 1 and supplementary Figs. S1 and S2).⁶⁰ The terminal BB and BO distances can be classified as single B—B and triple B≡O bonds,^{63–65} which are very similar for **1** and **2**. However, the BO distances within

the B_3O_3 ring differ markedly from **1** to **2**. In **2**, all these BO distances are roughly equal (1.37–1.38 Å), resulting in a nearly perfect hexagon. In sharp contrast, the BO distances within the B_3O_3 ring in **1** are highly uneven, ranging from “regular” distances for BO and BO (1.37 Å), to significantly elongated ones for BO and BO (1.48 Å), and to significantly shortened ones for BO and BO (1.28 Å); the latter value is rather close to a typical double B=O bond.⁶³ As a consequence, the hexagonal ring in **1** is structurally distorted. The situation is the same in C_6H_5^+ and C_6H_5 , where a single positive charge distorts the cationic structure (Fig. 1(d)).

Upon electron attachment, the three-dimensional $C_s \text{B}_5\text{O}_5^-$ (**3**) anion structure becomes the global minimum (Fig. 1(c)), in which the center B atom features tetrahedral hybridization, being terminated by three BO groups and one OBO unit. The B1B2, B1B3, and B1B4 distances (1.69 Å) are typical B—B single bonds, and the terminal BO groups can be assigned as B≡O triple bonds. The BO distances within the OBO unit are uneven: 1.23 Å versus 1.29 Å, which are close to the B≡O and B=O bonds, respectively.^{48,63} The B1-O5 bond should be roughly considered as a single bond, although the distance (1.51 Å) is markedly longer than a typical single bond; see Section IV B for further discussion. The $C_s \text{B}_5\text{O}_5^-$ (**3**) anion structure can be constructed from $T_d \text{B}(\text{BO})_4^-$ by inserting an O atom into one of the B—B σ bonds in the latter.⁴⁴

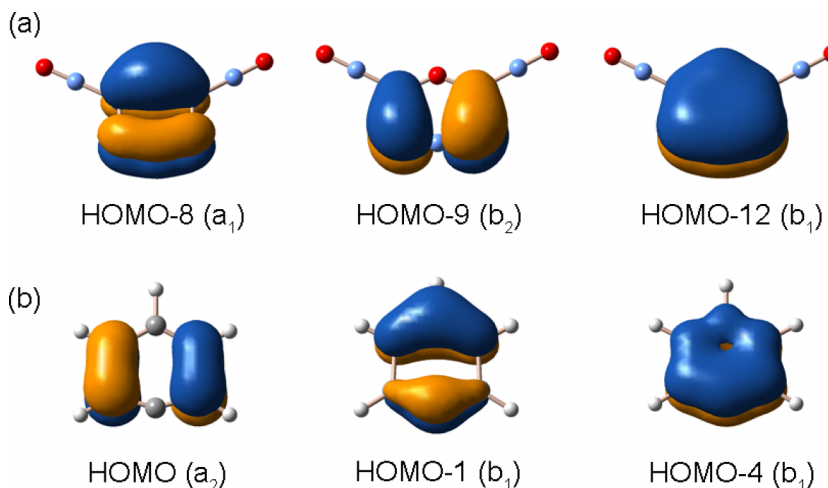


FIG. 2. Comparison of the π canonical molecular orbitals (CMOs) of (a) C_{2v} $B_5O_5^+$ (**1**) and (b) C_{2v} $C_6H_5^+$.

IV. DISCUSSION

A. Planar $B_3O_3(BO)_2^{+/0}$ clusters: Boron oxide analogs of hydrocarbons $C_6H_5^{+/0}$

The global-minimum structures **1** and **2** for $B_5O_5^{+/0}$ are rather similar (Fig. 1), except for the distortion of the B_3O_3 ring in **1**. Indeed, the electronic structure of the two species is nearly the same, which differs by a single electron. The lowest unoccupied molecular orbital (LUMO) of **1** becomes the single occupied molecular orbital (SOMO; supplementary Fig. S4)⁶⁰ in **2**. All other CMOs in **1** and **2** show one-to-one correspondence with each other. A boroxol B_3O_3 ring, such as that in D_{3h} B_6O_6 or D_{3h} $B_3O_3H_3$, is known to possess a π sextet,²⁸ which makes use of three O 2p lone pairs for three completely delocalized π bonds. These BO based species are therefore considered to be “inorganic benzenes”. The current **1** and **2** clusters provide new examples for this analogy. To be specific, **1** and **2** are comparable to phenyl cation ($C_6H_5^+$) and phenyl radical (C_6H_5), respectively (Fig. 1). Figure 2(a) depicts the three π CMOs of **1**, which are compared to those of $C_6H_5^+$ (Fig. 2(b)), showing close analogy between the two

species. Both of them possess a π sextet and are thus π aromatic, following the $(4n + 2)$ Hückel rule. Furthermore, our calculated nucleus-independent chemical shift (NICS) values, NICS(0)/NICS(1), for the B_3O_3 ring in **1** and **2** are $-5.12/-3.06$ and $-1.29/-2.61$ ppm, respectively, which are consistent with the nature of π aromaticity. Here, NICS(0) and NICS(1) are calculated at the center of the ring and at 1 Å above the center, respectively. It is stressed that aromaticity in the boroxol ring is relatively weak²⁸ with respect to that in the organic hydrocarbons, because the former originates from three O 2p lone pairs and the extent of delocalization is poor. For comparison, the NICS(0)/NICS(1) values are $-17.47/-11.97$ and $-11.19/-10.91$ ppm for $C_6H_5^+$ and C_6H_5 , respectively, at the same level of theory.

The SOMO of **2** (supplementary Fig. S4)⁶⁰ is mainly localized on the B1 atom in B_3O_3 ring, with very minor interactions with other atoms. Intuitively, when removing the single electron from this SOMO, the nature of bonding in the system should remain intact, except for a change in the natural charge on B1 (supplementary Fig. S5(a) versus supplementary Fig. S5(b)).⁶⁰ It is thus quite remarkable to observe a significant

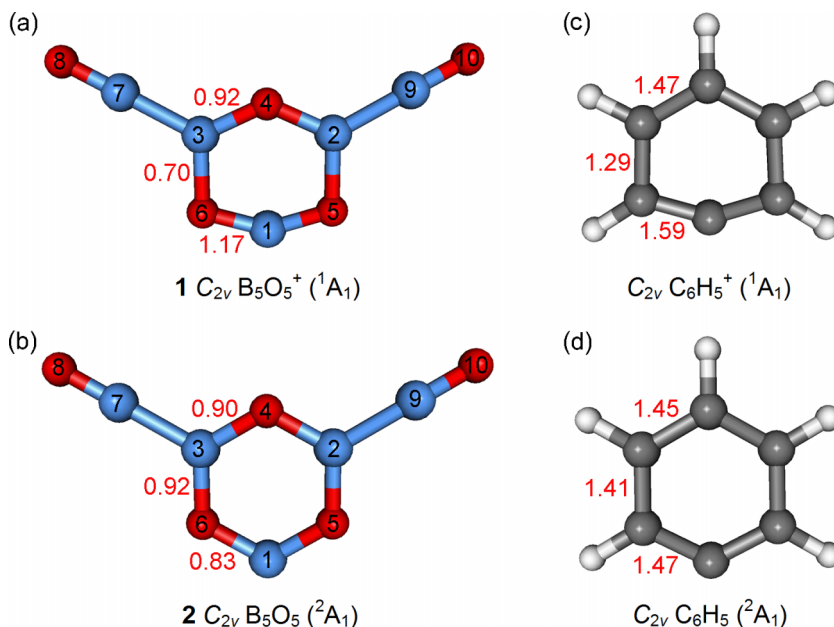


FIG. 3. Wiberg bond indices for (a) $B_5O_5^+$ (**1**) and (b) B_5O_5 (**2**), as compared to those of (c) $C_6H_5^+$ and (d) C_6H_5 . The B^+ or C^+ center in the cationic clusters results in unevenness of bond distances in the hexagonal cores.

structural change within the B_3O_3 ring between **1** and **2** (Fig. 1). As shown in Fig. 3(a), the calculated Wiberg bond indices within the B_3O_3 ring in **1** are highly uneven: 0.92, 0.70, and 1.17, the latter appearing to be beyond a typical single bond. These Wiberg bond indices are perfectly in line with their bond distances (Fig. 1(a)). We believe the unevenness and distortion of the ring are due to the highly positive nature of the B1 center in **1**, which is formally B^+ for the extra charge in B_5O_5^+ (supplementary Fig. S5(a)).⁶⁰ The B1 center is thus electrophilic and effectively attracts the O 2p electrons from O5 and O6, enhancing the BO and BO σ bonds while weakening the BO and BO σ bonds. The BO and BO σ bonds are “normal” and can serve as a reference for the unevenness. Not surprisingly, the same structural distortion occurs between C_6H_5 and C_6H_5^+ (Figs. 1 and 3). All other natural charges in **1**

and **2** (supplementary Fig. S5)⁶⁰ are consistent with the polar nature of B-O bonding: B +0.7 to +1.0 |e| and O -0.6 to -0.9 |e|, which are generally in line with previous data on the B_6O_6 cluster.²⁸

The AdNDP represents the bonding of a molecule in terms of n -center two-electron ($nc\text{-}2e$) bonds, with n ranging from one to the total number of atoms in the system. The AdNDP analysis thus includes the classical Lewis bonding elements (lone pairs and $2c\text{-}2e$ bonds), as well as the nonclassical delocalized $nc\text{-}2e$ bonds, which is particularly useful for the electron-deficient and aromatic clusters.⁵⁵ The AdNDP pattern of B_5O_5^+ (**1**) is shown in Fig. 4(a). A 2s/2p lone pair is revealed for every O center and each of the terminal BO group is associated with a $\text{B}\equiv\text{O}$ triple bond and a B—B single bond. This leaves a total of 18 valence electrons for bonding in

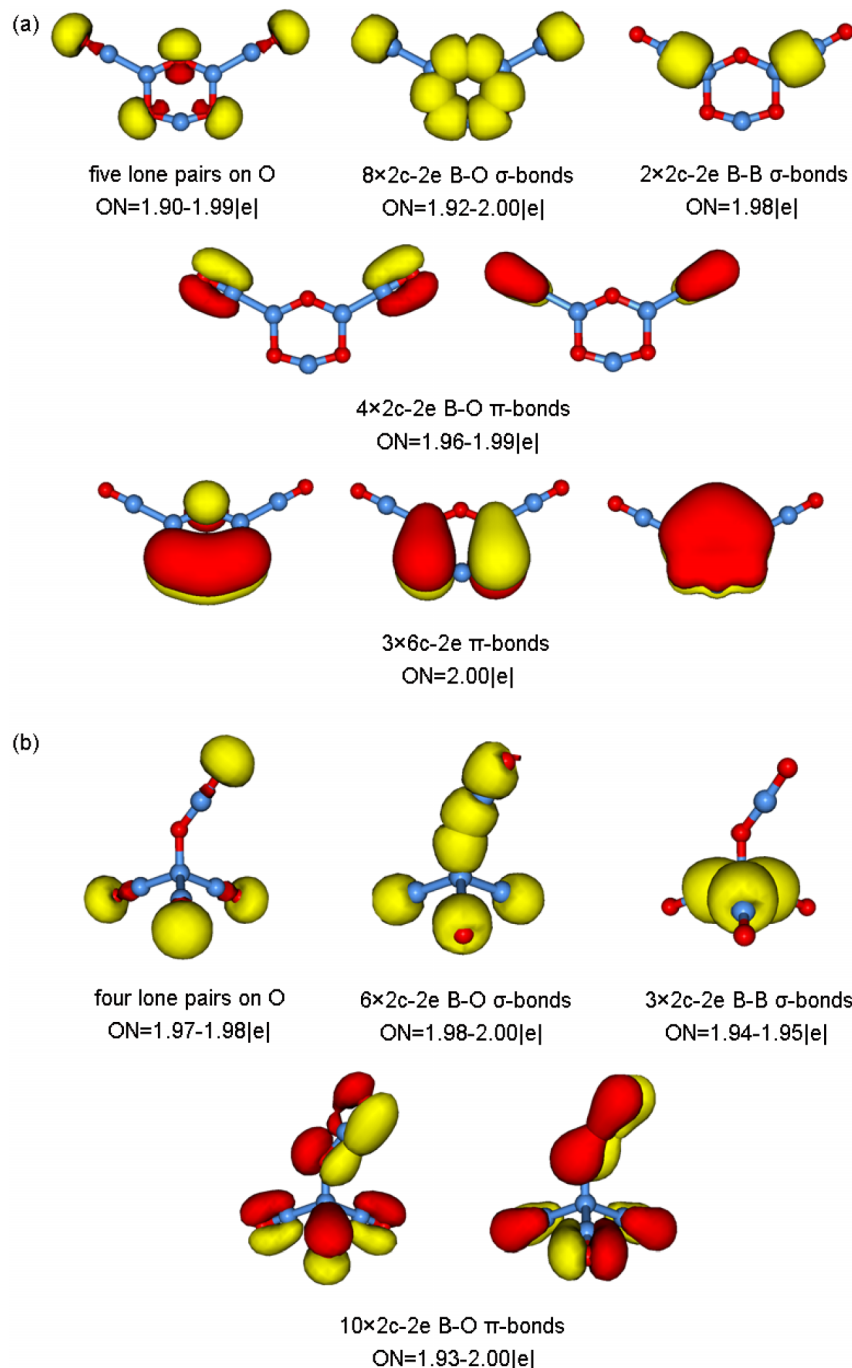
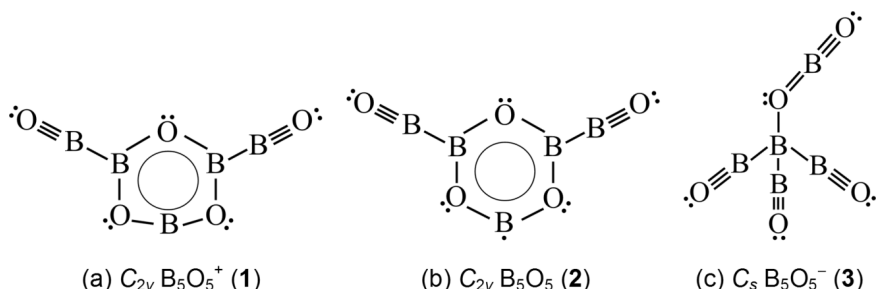


FIG. 4. AdNDP bonding patterns for (a) B_5O_5^+ (**1**, C_{2v}) and (b) B_5O_5^- (**3**, C_s). The occupation numbers (ONs) are shown. The lower BO σ “bond” within the OBO unit in **3** is not real and can be traced back to an O 2s lone pair; see text for details.



the B_3O_3 ring, 12 of which are used for the six 2c-2e $B—O$ σ bonds. The remaining 6 electrons are responsible for the global, delocalized π bonding (Fig. 4(a); the third row), which conform to the $(4n + 2)$ Hückel rule for aromaticity, consistent with the CMO analysis (Fig. 2(a)). The above bonding pattern for **1** is illustrated as the Lewis presentation in Fig. 5(a), where the circle represents the delocalized π sextet; a similar bonding pattern for **2** is shown in Fig. 5(b).

B. Tetrahedral $B_5O_5^-$ anion cluster: An analog of chloromethane and the dual 3c-4e π hyperbonds

Chloromethane (CH_3Cl ; Fig. 1(f)) is widely used in industrial manufacture and is always the favorite for scientists in experiment and theory.^{66–70} Simply speaking, the tetrahedral hybridized C in CH_3Cl forms four single covalent bonds with three H and one Cl. Delightedly, our global minimum $B_5O_5^-$ (**3**) can be considered as the boron oxide analog of CH_3Cl . Indeed, **3** is readily constructed from CH_3Cl based on the BO/H isolobal analogy and the isovalency between C and B^- (that is, the so-called “electronic transmutation”).^{33,38,39,44} The substitutional relationship between Cl and BO_2 unit is due to the fact that the latter is a well-known superhalogen with an electron affinity 4.46 eV.³³ Superhalogens are molecules whose electron affinities far exceed those of the halogens (Cl: 3.61 eV). NBO analysis shows that the tetrahedral hybridized B center in **3** carries a negative charge of $-0.64|e|$ (supplementary Fig. S5(c)).^{60–62} This is markedly different from other B centers, which carry positive charges (+0.9 to +1.2|e|). Additional negative charge is distributed on the OBO unit, whereas the BO groups are practically neutral. The NBO analysis thus clearly establishes a tetracoordinate B^- center in **3**.

The calculated bond distances (Fig. 1(c)) fully support the analogy between **3** and CH_3Cl . First, the BO groups possess the distances of 1.21 Å, which maintain the structural integrity as a boronyl ligand with $B\equiv O$ triple bond.²⁹ Second, the $B-(BO)$ distance, 1.69 Å, is typical for a $B-B$ single bond, consistent with the BO/H analogy as monovalent σ radicals. Third, the $B-(OBO)$ distance, 1.51 Å, may be roughly assigned as a $B-O$ single bond. The elongation of this $B-O$ single bond with respect to a typical one (~1.4 Å in **2**; Fig. 1(b)) is due to the intramolecular Coulomb repulsion, where both B and O are negatively charged ($-0.64|e|$ versus $-0.85|e|$; supplementary Fig. S5(c)).^{60–62} Note that B is the only B atom in **3** that carries a negative charge. The above assignments are based on the latest recommended atomic radii,⁶³ which give the upper limit of the $B\equiv O$ triple bond and $B=O$ double bond as 1.26 and 1.35 Å, respectively.

FIG. 5. Schematic Lewis presentations of the global-minimum structures in different charge states: (a) $B_5O_5^+$ (**1**, C_{2v}), (b) B_5O_5 (**2**, C_{2v}), and (c) $B_5O_5^-$ (**3**, C_s). The positive charge in **1** is located on the B atom at the bottom (B^+), whereas the extra negative charge in **3** is located on the tetracoordinate B center (B^-). The circle in (a) and (b) denotes the delocalized π sextet.

The OBO block in structure **3** possesses asymmetric BO distances of 1.23 Å versus 1.29 Å. The shorter distance is typical for a $B\equiv O$ triple bond,²⁹ while the longer is consistent with a $B=O$ double bond,⁶³ as illustrated in the approximate Lewis structure (Fig. 5(c)). Key CMOs that are responsible for the OBO bonding in **3** are depicted in supplementary Fig. S6.⁶⁰ Although these CMOs are highly mixed in nature, their contribution to the bonding in the OBO unit can be roughly analyzed. Here, the highest occupied molecular orbital (HOMO) and HOMO – 14 are derived from $2p_z$ atomic orbitals (AOs) of O_5/O_7 . The former is essentially nonbonding within the OBO unit, with 28% and 26% $O 2p_z$ contribution from the two O centers; whereas the latter is a completely bonding π CMO. HOMO and HOMO – 14 thus form a 3c-4e π hyperbond for the OBO unit in the p_z manifold, which is reminiscent of the prototypical 3c-4e σ hyperbond (ω -bond) in XeF_2 or FHF^- .⁷¹ It is noted that our 3c-4e hyperbond is a π bond in the p_z manifold, while that in XeF_2 and FHF^- is a σ bond. Concurrently, the bonding/nonbonding combination of HOMO – 1 and HOMO – 15 forms another 3c-4e π hyperbond for the OBO unit, which is responsible for bonding in the p_y manifold: HOMO – 1 is contributed from O_7 (22%) and O_5 (19%) with negligible contribution from B_6 , whereas HOMO – 15 is completely bonding. These two sets of bonding/nonbonding combinations define the dual 3c-4e π hyperbonds in **3**. In addition, HOMO – 10 represents the B_6-O_7 σ bond. In summary, the dual 3c-4e π hyperbonds and the B_6-O_7 σ bond collectively generate the triple $B_6\equiv O_7$ and double $B_6=O_5$ bonds in **3**, which are consistent with their bond distances (1.23/1.29 Å). NBO analysis indicates that the Wiberg bond indices for three terminal BO groups in **3** are 1.81, compared to 1.70/1.07 for the BO bonds within the OBO unit, which are in line with the CMO analysis and the bond distances.

The above bonding picture for **3** is basically born out from the AdNDP analysis.⁵⁵ As shown in Fig. 4(b), three $B-B$ σ bonds (B_1-B_2 , B_1-B_3 , and B_1-B_4), three 2c-2e terminal $B\equiv O$ triple bonds ($B_2\equiv O_8$, $B_3\equiv O_9$, and $B_4\equiv O_{10}$), and another $B-O$ σ bond (B_1-O_5) are revealed, as are the lone pairs on the four terminal O centers. In terms of the bonding within the OBO unit, the AdNDP results clearly recover the $B_6\equiv O_7$ triple bond. It appears that the AdNDP data for the bonding between B_6 and O_5 are different from the CMO analysis, with the former also suggesting a $B\equiv O$ bond between B_6 and O_5 . When tracing back the B_6-O_5 σ “bond” to the CMO, we can resolve this contradiction easily. The corresponding CMO is in fact based on the $O 2s$ AO from the O_5 atom (83%), nearly identical to the $O 2s$ lone pairs on the O_7 , O_8 , O_9 , and O_{10} atoms (95%, 86%, 86%, and 83%, respectively). Hence,

the B6—O5 σ “bond” in AdNDP is actually an O 2s lone pair and the BO bonding should be viewed as a double bond, as illustrated in Fig. 5(c).

Finally, the global-minimum structural changes from cation/neutral (**1/2**) to anion (**3**) (Fig. 1) are quite interesting, which demonstrates the close interplay between the B≡O, OBO, B—O, B—B, and boroxol ring in the chemical bonding in $\text{B}_5\text{O}_5^{+/0/-}$. In these electron-deficient boron oxide clusters, every electron counts and a single electron can make a difference. We believe the key to the energetic reverse of **2** as global minimum for B_5O_5 neutral versus **3** as global minimum for B_5O_5^- anion lies in the nature of their frontier CMOs: The LUMO of the hexagonal isomer of B_5O_5 is B based and primarily localized (supplementary Fig. S4),⁶⁰ whereas that of the tetrahedral isomer is O based and fully delocalized (supplementary Fig. S6).⁶⁰ Adding a single electron to either the B based or O based orbital is anticipated to make a huge difference of up to a couple of eV for the anion isomers, leading to enhanced stability for the tetrahedral anion.

C. Predicted vibrational and electronic properties of $\text{B}_5\text{O}_5^{+/0/-}$

The calculated IR absorption spectra of $\text{B}_5\text{O}_5^{+/0/-}$ clusters are shown in supplementary Fig. S7,⁶⁰ which should facilitate the forthcoming experimental characterizations of these clusters. The intensities of most IR active modes are very weak. For cationic B_5O_5^+ (**1**), the main features are four characteristic vibrational peaks at 1840 (b₂), 1337 (b₂), 1178 (a₁), and 1017 (a₁) cm⁻¹. For the neutral B_5O_5 (**2**), which also features a boroxol B_3O_3 ring, only the two modes at 1367 (b₂) and 1350 (a₁) cm⁻¹ exhibit strong intensities. Note that the strongest vibrations for both **1** and **2** are associated with the B_3O_3 core, which is the main skeleton of the structures. As a result of the distinct structural difference between $\text{B}_5\text{O}_5^{+/0}$ (**1, 2**) and B_5O_5^- (**3**), it is easy to differentiate between the B_5O_5^- and $\text{B}_5\text{O}_5^{+/0}$ clusters on the basis of their vibrational modes (supplementary Fig. S7(a)/S7(b) versus supplementary Fig. S7(c)).⁶⁰ According to our calculations, the main modes for **3** are due to the stretching vibrations of the four terminal BO units, 2043 (a'), 1940 (a'), 1926 (a''), and 1926 (a') cm⁻¹. The first a' mode is predominant.

Photoelectron spectroscopy (PES) is a powerful tool to characterize anion clusters. The ground-state adiabatic and vertical detachment energies (ADE and VDE) of **3** are calculated to be ADE/VDE = 6.28/6.77 eV at the B3LYP level and 6.42/7.19 eV at the single-point CCSD(T) level. The higher VDEs for excited-state transitions are also predicted using the TD-B3LYP method. A simulated photoelectron spectrum of **3** is shown in Fig. 6. Overall, the spectrum shows extremely high electron binding energies, implying a remarkably stable anion cluster for **3**.

Note that a potential, competitive isomeric structure for B_5O_5^- anion cluster is C_{2v} ($^1\text{A}_1$) (supplementary Fig. S3),⁶⁰ which is ~2 kcal/mol above the global minimum **3** at the single-point CCSD(T) level. This isomer has a rhombic B_2O_2 core with three terminal B≡O groups, whose bond distances and natural charges are shown in supplementary Fig. S8.⁶⁰ The key bonding elements based on CMO and AdNDP analyses

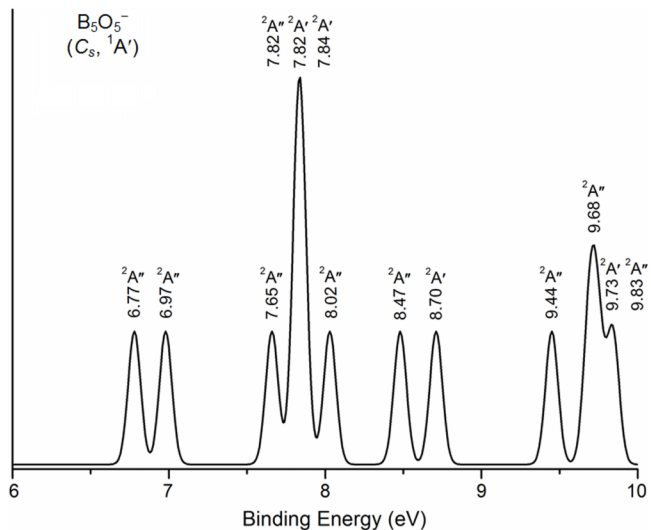


FIG. 6. Simulated photoelectron spectrum of the anion global-minimum, B_5O_5^- (**3**), on the basis of TD-B3LYP calculations. The labelled states are the ground state and excited states of the corresponding tetrahedral neutral species. The simulations were done by fitting the distribution of the calculated VDEs with unit-area Gaussian functions of 0.04 eV half-width.

are presented in supplementary Fig. S9.⁶⁰ The rhombic B_2O_2 core features a 4c-4e π bond (supplementary Fig. S9(a)),⁶⁰ due to the HOMO – 1/HOMO – 13 combination. Here, HOMO – 13 is delocalized and completely bonding, whereas HOMO – 1 is essentially nonbonding. Such a nonbonding/bonding system is recently described as an o-bond.^{46,48} The o-bond differs from a typical 4π antiaromatic system; the latter features an antibonding/bonding combination for the two π CMOs, which leads to a rectangular structural distortion. The HOMO of C_{2v} ($^1\text{A}_1$) is also localized around the tetracoordinate B atom, suggesting an approximate “B⁻” center. Indeed, the calculated natural charge on this B center (+0.06 |e|) is the smallest of all B centers, compared to the “normal” values of +0.65/ + 0.79/ + 0.86 |e| on other B atoms. The calculated first VDE is 6.54 eV at the B3LYP level, which is smaller than that of the global-minimum structure **3**.

D. Growth pattern of the whole B_nO_n ($n = 1$ –6) series

The current $\text{B}_5\text{O}_5^{+/0/-}$ clusters complete the B_nO_n ($n = 1$ –6) series. The structures of $\text{B}_n\text{O}_n^{0/-}$ ($n = 1, 2$) clusters were studied sufficiently in the past years.^{31–33} Boronyl boroxine, D_{3h} B_6O_6 [$\text{B}_3\text{O}_3(\text{BO})_3$], is a boron oxide analog of boroxine and benzene, which was reported in 2013.²⁸ Subsequently, we reported a computational study on the structural and bonding properties of a series of $\text{B}_3\text{O}_n^{-/0/+}$ ($n = 2$ –4) clusters, as well as a joint experimental and theoretical study on the $\text{B}_4\text{O}_4^{0/-}$ clusters.^{46,48} Now it is time to discuss the structural and bonding evolution along the whole B_nO_n ($n = 1$ –6) series. Figure 7 summarizes the structures and cohesive energies of these clusters. The cluster structures follow this trend: linear clusters (BO and B_2O_2) → structures containing a B_2O_2 rhombic ring (B_3O_3 and B_4O_4) → structures with a boroxol core (B_5O_5 and B_6O_6). The terminal BO groups feature the B≡O triple bonds, the BB bonding is single σ bond in nature, whereas the rhombic or hexagonal rings are held together by B—O single bonds.

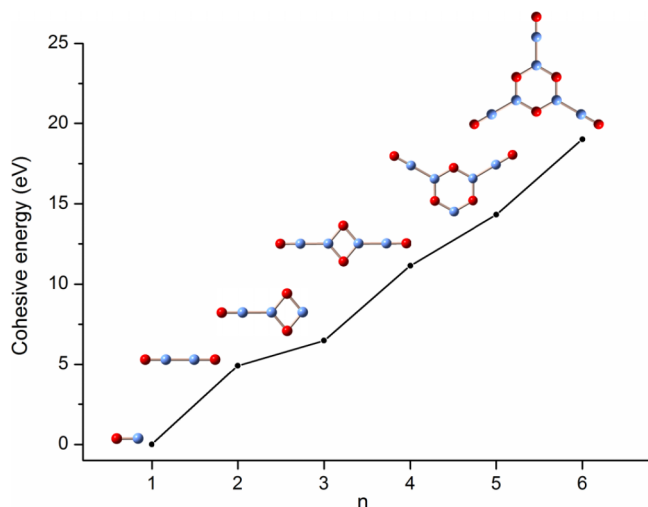


FIG. 7. Calculated cohesive energy for B_nO_n ($n = 1\text{--}6$) clusters at the B3LYP level, as a function of cluster size n . The optimized global-minimum structures are shown. The cohesive energy is evaluated with respect to n $B\equiv O$ groups.

In fact, all these B_nO_n clusters are readily constructed from n $B\equiv O$ groups. To form a B_nO_n cluster, the n th $B\equiv O$ group may attach straightforwardly to $B_{n-1}O_{n-1}$ via a $B-B$ single bond. The n th $B\equiv O$ group may also be converted to two $B-O$ single bonds, which combine with another $B\equiv O$ group for a rhombic B_2O_2 unit and concurrently generates two O 2p lone pairs; the latter can further delocalize for a 4c-4e π bond (that is, the o-bond). Alternatively, the n th $B\equiv O$ group may be inserted into the core BO ring, expanding the latter in size and contributing an extra O 2p lone pair for delocalized π bonding in the new core.

In terms of the cohesive energy of a B_nO_n cluster with respect to n BO groups, the size trend follows a rough linear relationship (Fig. 7). We can calculate the normalized coefficient and the expression is as follows: $E = 3.86n - 3.48$ ($n = 1\text{--}6$; with standard slope error of 0.20). Meanwhile, the expressions for the odd and even species are $E = 3.58n - 3.81$ ($n = 1, 3, 5$) and $E = 3.52n - 2.41$ ($n = 2, 4, 6$), with a standard slope error of 0.20 and 0.23, respectively. The average cohesive energy per BO group is evaluated to be ~ 3.8 eV. Notably, the cohesive energy increases sharply at B_2O_2 , B_4O_4 , and B_6O_6 , suggesting enhanced electronic and/or structural stabilities for these clusters.

V. CONCLUSIONS

In conclusion, we report on theoretical predictions of the global-minimum structures and chemical bonding of a series of boron oxide clusters, $B_5O_5^{+/-}$ (**1–3**), at the B3LYP and single-point CCSD(T) levels. The planar $B_5O_5^{+/-}$ (**1, 2**) clusters feature a boroxol ring as core with two terminal boronyl groups, which are shown to be close inorganic analogs of $C_6H_5^{0/+}$. The three-dimensional $B_5O_5^-$ (**3**) anion cluster has a tetrahedral B^- center, terminated with three boronyls and one OBO group, analogous to chloromethane (CH_3Cl). Chemical bonding analyses reveal dual three-center four-electron (3c-4e) π hyperbonds in **3**. It is interesting that a single electron

can markedly change the structural and electronic properties of a molecular system, turning the species from an analog of $C_6H_5^{+/-}$ to that of CH_3Cl . The present results offer new examples for the structural and chemical analogy between electron-deficient boron oxide clusters and hydrocarbons. Such clusters may be generated directly in the gas phase under appropriate oxidizing conditions using the laser vaporization technique. Alternatively, they may be produced using boronyl boroxine as the precursor, provided that the latter is available as a gas-phase cluster or synthetic compound.

ACKNOWLEDGMENTS

This work was supported by the National Natural Science Foundation of China (Grant Nos. 21243004 and 21373130), the Shanxi International Cooperation project (Grant No. 2013081018), and the State Key Laboratory of Quantum Optics and Quantum Optics Devices (Grant No. KF201402). H.J.Z. gratefully acknowledges the start-up fund from Shanxi University for support.

- ¹H. J. Zhai, L. S. Wang, A. N. Alexandrova, and A. I. Boldyrev, *J. Phys. Chem. A* **107**, 9319 (2003).
- ²H. J. Zhai, L. S. Wang, A. N. Alexandrova, and A. I. Boldyrev, *J. Chem. Phys.* **117**, 7917 (2002).
- ³A. N. Alexandrova, A. I. Boldyrev, H. J. Zhai, L. S. Wang, E. Steiner, and P. W. Fowler, *J. Phys. Chem. A* **107**, 1359 (2003).
- ⁴A. N. Alexandrova, A. I. Boldyrev, H. J. Zhai, and L. S. Wang, *J. Phys. Chem. A* **108**, 3509 (2004).
- ⁵H. J. Zhai, A. N. Alexandrova, K. A. Birch, A. I. Boldyrev, and L. S. Wang, *Angew. Chem., Int. Ed.* **42**, 6004 (2003).
- ⁶A. N. Alexandrova, H. J. Zhai, L. S. Wang, and A. I. Boldyrev, *Inorg. Chem.* **43**, 3552 (2004).
- ⁷H. J. Zhai, B. Kiran, J. Li, and L. S. Wang, *Nat. Mater.* **2**, 827 (2003).
- ⁸A. P. Sergeeva, D. Y. Zubarev, H. J. Zhai, A. I. Boldyrev, and L. S. Wang, *J. Am. Chem. Soc.* **130**, 7244 (2008).
- ⁹A. N. Alexandrova, A. I. Boldyrev, H. J. Zhai, and L. S. Wang, *J. Chem. Phys.* **122**, 054313 (2005).
- ¹⁰C. Romanescu, D. J. Harding, A. Fielicke, and L. S. Wang, *J. Chem. Phys.* **137**, 014317 (2012).
- ¹¹W. Huang, A. P. Sergeeva, H. J. Zhai, B. B. Averkiev, L. S. Wang, and A. I. Boldyrev, *Nat. Chem.* **2**, 202 (2010).
- ¹²B. Kiran, S. Bulusu, H. J. Zhai, S. Yoo, X. C. Zeng, and L. S. Wang, *Proc. Natl. Acad. Sci. U. S. A.* **102**, 961 (2005).
- ¹³A. N. Alexandrova, A. I. Boldyrev, H. J. Zhai, and L. S. Wang, *Coord. Chem. Rev.* **250**, 2811 (2006).
- ¹⁴Z. A. Piazza, W. L. Li, C. Romanescu, A. P. Sergeeva, L. S. Wang, and A. I. Boldyrev, *J. Chem. Phys.* **136**, 104310 (2012).
- ¹⁵A. P. Sergeeva, Z. A. Piazza, C. Romanescu, W. L. Li, A. I. Boldyrev, and L. S. Wang, *J. Am. Chem. Soc.* **134**, 18065 (2012).
- ¹⁶I. A. Popov, Z. A. Piazza, W. L. Li, L. S. Wang, and A. I. Boldyrev, *J. Chem. Phys.* **139**, 144307 (2013).
- ¹⁷Z. A. Piazza, I. A. Popov, W. L. Li, R. Pal, X. C. Zeng, A. I. Boldyrev, and L. S. Wang, *J. Chem. Phys.* **141**, 034303 (2014).
- ¹⁸W. L. Li, Y. F. Zhao, H. S. Hu, J. Li, and L. S. Wang, *Angew. Chem., Int. Ed.* **53**, 5540 (2014).
- ¹⁹W. L. Li, Q. Chen, W. J. Tian, H. Bai, Y. F. Zhao, H. S. Hu, J. Li, H. J. Zhai, S. D. Li, and L. S. Wang, *J. Am. Chem. Soc.* **136**, 12257 (2014).
- ²⁰Z. A. Piazza, H. S. Hu, W. L. Li, Y. F. Zhao, J. Li, and L. S. Wang, *Nat. Commun.* **5**, 3113 (2014).
- ²¹Q. Chen, G. F. Wei, W. J. Tian, H. Bai, Z. P. Liu, H. J. Zhai, and S. D. Li, *Phys. Chem. Chem. Phys.* **16**, 18282 (2014).
- ²²H. J. Zhai, Y. F. Zhao, W. L. Li, Q. Chen, H. Bai, H. S. Hu, Z. A. Piazza, W. J. Tian, H. G. Lu, Y. B. Wu, Y. W. Mu, G. F. Wei, Z. P. Liu, J. Li, S. D. Li, and L. S. Wang, *Nat. Chem.* **6**, 727 (2014).
- ²³Q. Chen, W. L. Li, Y. F. Zhao, S. Y. Zhang, H. S. Hu, H. Bai, H. R. Li, W. J. Tian, H. G. Lu, H. J. Zhai, S. D. Li, J. Li, and L. S. Wang, *ACS Nano* **9**, 754 (2015).
- ²⁴I. Boustani, A. Rubio, and J. A. Alonso, *Chem. Phys. Lett.* **311**, 21 (1999).

- ²⁵F. Y. Tian and Y. X. Wang, *J. Chem. Phys.* **129**, 024903 (2008).
- ²⁶W. L. Li, C. Romanescu, T. Jian, and L. S. Wang, *J. Am. Chem. Soc.* **134**, 13228 (2012).
- ²⁷D. Z. Li, Q. Chen, Y. B. Wu, H. G. Lu, and S. D. Li, *Phys. Chem. Chem. Phys.* **14**, 14769 (2012).
- ²⁸D. Z. Li, H. Bai, Q. Chen, H. G. Lu, H. J. Zhai, and S. D. Li, *J. Chem. Phys.* **138**, 244304 (2013).
- ²⁹H. J. Zhai, Q. Chen, H. Bai, S. D. Li, and L. S. Wang, *Acc. Chem. Res.* **47**, 2435 (2014).
- ³⁰D. Peiris, A. Lapicki, S. L. Anderson, R. Napora, D. Linder, and M. Page, *J. Phys. Chem. A* **101**, 9935 (1997).
- ³¹T. R. Burkholder and L. Andrews, *J. Chem. Phys.* **95**, 8697 (1991).
- ³²M. L. Drummond, V. Meunier, and B. G. Sumpter, *J. Phys. Chem. A* **111**, 6539 (2007).
- ³³H. J. Zhai, L. M. Wang, S. D. Li, and L. S. Wang, *J. Phys. Chem. A* **111**, 1030 (2007).
- ³⁴T. B. Tai and M. T. Nguyen, *Chem. Phys. Lett.* **483**, 35 (2009).
- ³⁵M. T. Nguyen, M. H. Matus, V. T. Ngan, D. J. Grant, and D. A. Dixon, *J. Phys. Chem. A* **113**, 4895 (2009).
- ³⁶T. B. Tai, M. T. Nguyen, and D. A. Dixon, *J. Phys. Chem. A* **114**, 2893 (2010).
- ³⁷C. B. Shao, L. Jin, and Y. H. Ding, *J. Comput. Chem.* **32**, 771 (2011).
- ³⁸H. J. Zhai, S. D. Li, and L. S. Wang, *J. Am. Chem. Soc.* **129**, 9254 (2007).
- ³⁹S. D. Li, H. J. Zhai, and L. S. Wang, *J. Am. Chem. Soc.* **130**, 2573 (2008).
- ⁴⁰H. J. Zhai, J. C. Guo, S. D. Li, and L. S. Wang, *ChemPhysChem* **12**, 2549 (2011).
- ⁴¹H. J. Zhai, C. Q. Miao, S. D. Li, and L. S. Wang, *J. Phys. Chem. A* **114**, 12155 (2010).
- ⁴²H. Bai, H. J. Zhai, S. D. Li, and L. S. Wang, *Phys. Chem. Chem. Phys.* **15**, 9646 (2013).
- ⁴³Q. Chen, H. J. Zhai, S. D. Li, and L. S. Wang, *J. Chem. Phys.* **137**, 044307 (2012).
- ⁴⁴W. Z. Yao, J. C. Guo, H. G. Lu, and S. D. Li, *J. Phys. Chem. A* **113**, 2561 (2009).
- ⁴⁵R. J. Doyle, Jr., *J. Am. Chem. Soc.* **110**, 4120 (1988).
- ⁴⁶Q. Chen, H. G. Lu, H. J. Zhai, and S. D. Li, *Phys. Chem. Chem. Phys.* **16**, 7274 (2014).
- ⁴⁷W. J. Tian, H. G. Xu, X. Y. Kong, Q. Chen, W. J. Zheng, H. J. Zhai, and S. D. Li, *Phys. Chem. Chem. Phys.* **16**, 5129 (2014).
- ⁴⁸W. J. Tian, L. J. Zhao, Q. Chen, T. Ou, H. G. Xu, W. J. Zheng, H. J. Zhai, and S. D. Li, *J. Chem. Phys.* **142**, 134305 (2015).
- ⁴⁹A. P. Sergeeva, B. B. Averkiev, H. J. Zhai, A. I. Boldyrev, and L. S. Wang, *J. Chem. Phys.* **134**, 224304 (2011).
- ⁵⁰M. Saunders, *J. Comput. Chem.* **25**, 621 (2004).
- ⁵¹R. A. Kendall, T. H. Dunning, Jr., and R. J. Harrison, *J. Chem. Phys.* **96**, 6796 (1992).
- ⁵²J. Čížek, *Adv. Chem. Phys.* **14**, 35 (1969).
- ⁵³G. E. Scuseria and H. F. Schaefer III, *J. Chem. Phys.* **90**, 3700 (1989).
- ⁵⁴R. J. Bartlett and M. Musial, *Rev. Mod. Phys.* **79**, 291 (2007).
- ⁵⁵D. Y. Zubarev and A. I. Boldyrev, *Phys. Chem. Chem. Phys.* **10**, 5207 (2008).
- ⁵⁶E. D. Glendening, J. K. Badenhoop, A. E. Reed, J. E. Carpenter, J. A. Bohmann, C. M. Morales, and F. Weinhold, NBO 5.0, Theoretical Chemistry Institute, University of Wisconsin, Madison, 2001.
- ⁵⁷M. E. Casida, C. Jamorski, K. C. Casida, and D. R. Salahub, *J. Chem. Phys.* **108**, 4439 (1998).
- ⁵⁸R. Bauernschmitt and R. Ahlrichs, *Chem. Phys. Lett.* **256**, 454 (1996).
- ⁵⁹M. J. Frisch *et al.*, GAUSSIAN 09, Revision D.01, Gaussian, Inc. Wallingford, CT, 2009.
- ⁶⁰See supplementary material at <http://dx.doi.org/10.1063/1.4928282> for the Cartesian coordinates for the global-minimum $B_5O_5^{+/0/-}$ (**1–3**) structures at the B3LYP/aug-cc-pVTZ level; alternative low-lying isomers of $B_5O_5^{+/0/-}$ and their relative energies; comparison of π canonical molecular orbitals of B_5O_5 (**2**) and C_6H_5 ; natural charge distribution for the global minima of $B_5O_5^{+/0/-}$ (**1–3**); key bonding elements for $B_5O_5^-$ (**3**) as revealed from the canonical molecular orbital analyses; calculated infrared absorption spectra for $B_5O_5^{+/0/-}$ (**1–3**); and optimized structure of the second lowest-lying C_{2v} $B_5O_5^-$ isomer at the B3LYP/aug-cc-pVTZ level, its natural charge distribution, and its bonding pattern as revealed from AdNDP analysis.
- ⁶¹Extensive prior theoretical works on boron oxide clusters indicate that the natural charges at the density-functional theory levels from natural bond orbital (NBO) analysis are reliable, at least qualitatively. We note that the reported charge distribution herein is in line with chemical intuition, as well as with the chemical bonding analyses. This situation appears to be very different from that in the transition metal systems.⁶²
- ⁶²G. J. Cao, W. H. E. Schwarz, and J. Li, *Inorg. Chem.* **54**, 3695 (2015).
- ⁶³P. Pyykö and M. Atsumi, *Chem. - Eur. J.* **15**, 12770 (2009).
- ⁶⁴A. Moezzi, R. A. Bartlett, and P. P. Power, *Angew. Chem., Int. Ed. Engl.* **31**, 1082 (1992).
- ⁶⁵A. Moezzi, M. M. Olmstead, and P. P. Power, *J. Am. Chem. Soc.* **114**, 2715 (1992).
- ⁶⁶X. G. Zhao, S. C. Tucker, and D. G. Truhlar, *J. Am. Chem. Soc.* **113**, 826 (1991).
- ⁶⁷H. J. Böhm, R. Ahlrichs, P. Scharf, and H. Schiffer, *J. Chem. Phys.* **81**, 1389 (1984).
- ⁶⁸G. Lu, A. Linsebigler, and J. T. Yates, Jr., *J. Phys. Chem.* **99**, 7626 (1995).
- ⁶⁹T. N. Truong and E. V. Stefanovich, *J. Phys. Chem.* **99**, 14700 (1995).
- ⁷⁰D. C. Clary and J. Palma, *J. Chem. Phys.* **106**, 575 (1997).
- ⁷¹F. Weinhold and C. R. Landis, *Valency and Bonding: A Natural Bond Orbital Donor-Acceptor Perspective* (Cambridge University Press, Cambridge, 2005).